Journal of Pharmaceutical Analysis 15 (2025) 101039

Contents lists available at ScienceDirect

Journal of Pharmaceutical Analysis

journal homepage: www.elsevier.com/locate/jpa

Original article

Coral calcium hydride promotes peripheral mitochondrial division and reduces AT-II cells damage in ARDS via activation of the Trx2/Myo19/Drp1 pathway

Qian Li [a, b, 1], Yang Ang [b, c, 1], Qing-Qing Zhou [b, 1], Min Shi [d, 1], Wei Chen [e], Yujie Wang [e], Pan Yu [e], Bing Wan [b], Wanyou Yu [b], Liping Jiang [b], Yadan Shi [b], Zhao Lin [b], Shaozheng Song [f], Manlin Duan [g], Yun Long [b, *], Qi Wang [b, **], Wentao Liu [h, ***], Hongguang Bao [a, f, ****]

[a] Department of Anesthesiology, Nanjing First Hospital, Nanjing Medical University, Nanjing, 210000, China
[b] Department of Anesthesiology, Jiangning Hospital Affiliated to Nanjing Medical University, Nanjing, 211100, China
[c] Department of Anesthesiology, Nanjing Hospital of Chinese Medicine Affiliated to Nanjing University of Chinese Medicine, Nanjing, 211100, China
[d] Department of Anesthesiology, the First Affiliated Hospital of Naval Medical University, Shanghai, 200433, China
[e] Jinling College Affiliated to Nanjing Medical University, Nanjing, 211100, China
[f] Wuxi Taihu University, Wuxi, Jiangsu, 214064, China
[g] Department of Anesthesiology, BenQ Medical Center, The Affiliated BenQ Hospital of Nanjing Medical University, Nanjing, 210019, China
[h] Jiangsu Key Laboratory of Neurodegeneration, Department of Pharmacology, Nanjing Medical University, Nanjing, 211166, China

ARTICLE INFO

Article history:
Received 19 December 2023
Received in revised form
13 June 2024
Accepted 7 July 2024
Available online 18 July 2024

Keywords:
Coral calcium hydrogenation
ARDS
Mitochondria
Peripheral division
Trx2

ABSTRACT

Acute respiratory distress syndrome (ARDS) is a common respiratory emergency, but current clinical treatment remains at the level of symptomatic support and there is a lack of effective targeted treatment measures. Our previous study confirmed that inhalation of hydrogen gas can reduce the acute lung injury of ARDS, but the application of hydrogen has flammable and explosive safety concerns. Drinking hydrogen-rich liquid or inhaling hydrogen gas has been shown to play an important role in scavenging reactive oxygen species and maintaining mitochondrial quality control balance, thus improving ARDS in patients and animal models. Coral calcium hydrogenation (CCH) is a new solid molecular hydrogen carrier prepared from coral calcium (CC). Whether and how CCH affects acute lung injury in ARDS remains unstudied. In this study, we observed the therapeutic effect of CCH on lipopolysaccharide (LPS) induced acute lung injury in ARDS mice. The survival rate of mice treated with CCH and hydrogen inhalation was found to be comparable, demonstrating a significant improvement compared to the untreated ARDS model group. CCH treatment significantly reduced pulmonary hemorrhage and edema, and improved pulmonary function and local microcirculation in ARDS mice. CCH promoted mitochondrial peripheral division in the early course of ARDS by activating mitochondrial thioredoxin 2 (Trx2), improved lung mitochondrial dysfunction induced by LPS, and reduced oxidative stress damage. The results indicate that CCH is a highly efficient hydrogen-rich agent that can attenuate acute lung injury of ARDS by improving the mitochondrial function through Trx2 activation.

1. Introduction

The American Thoracic Society International Conference defined acute respiratory distress syndrome (ARDS) as generalized acute inflammatory lung injury caused by pulmonary or systemic factors [1]. The current mortality rate among ARDS patients remains alarmingly high (35%–45%), imposing a substantial medical burden on society [2]. European Society of Intensive Care Medicine (ESICM) guidelines on ARDS recommend improving ventilation and oxygenation, supportive therapy and steroid drug application [3].

* Corresponding author.
** Corresponding author.
*** Corresponding author.
**** Corresponding author. Department of Anesthesiology, Nanjing First Hospital, Nanjing Medical University, Nanjing, 210000, China.
E-mail addresses: longyun2001@hotmail.com (Y. Long), 19951957195@163.com (Q. Wang), painresearch@njmu.edu.cn (W. Liu), hongguang_bao@163.com (H. Bao).
Peer review under responsibility of Xi'an Jiaotong University.
[1] These authors contributed equally to this work.

https://doi.org/10.1016/j.jpha.2024.101039

The therapeutic targeting of the above measures is insufficient, and the precise treatment of ARDS needs to be further explored. The typical histological features of ARDS are diffuse alveolar injury, mainly manifested by pulmonary edema, inflammation, and alveolar hemorrhage [4]. Type II alveolar epithelial (AT II) cells, which have the ability to remove alveolar water, repair after injury, and proliferation and differentiation of alveolar stem cells, are the main participants in the development of ARDS [5]. Therefore, how to avoid damage to AT II cells and ensure their control function is an important direction of ARDS treatment.

Mitochondrial dysfunction caused by an imbalance of reactive oxygen species (ROS) is an important cause of AT II cell damage and ultimately leads to ARDS [6]. The body can completely clear the damaged mitochondria through autophagy, efferocytosis and other mechanisms to alleviate mitochondrial dysfunction [7]. Further studies revealed that the damaged mitochondrial DNA (mt DNA) could be clustered to one side at the initial stage of damage by means of peripheral division of the mitochondria, which is a type of quality control for partial mitochondrial clearance [8]. This mitochondrial quality control mechanism can promote removal of damaged mitochondria by regulating activation of the key proteins myosin 19 (Myo19) and dynamin-related protein 1 (Drp1) in the early stage of oxidative stress, reducing the damage caused by ROS and delaying ARDS progression [9]. Therefore, early promotion of mitochondrial peripheral division in the course of ARDS is important for protecting alveolar epithelial cells and reducing acute lung injury in ARDS.

Hydrogen has been an effective treatment for acute lung injury of ARDS in recent years [10]. Our previous experiments have confirmed that hydrogen has selective antioxidative and anti-inflammatory functions, and a strong penetrating ability; therefore, hydrogen can quickly cross the cell membrane and exert a biological effect [11]. While hydrogen has good biological effects, its flammable and explosive chemical properties limit its application. Coral calcium hydrogenation (CCH) is a new solid molecular hydrogen carrier prepared from coral calcium (CC). In the high temperature and high pressure state without oxygen, hydrogen is polarized in the plasma state to yield negative hydrogen ions. Negative hydrogen ions are absorbed into the crystal lattice and micropores of oyster calcium and magnesium in the state of polarization and ionization, and form negative hydrogen ionophores that are stable at room temperature. In the low oxygen partial pressure environment in the body, after CCH encounters water, it is converted into Ca^{2+}, Mg^{2+} and H^{-} and continues to release hydrogen [12]. Hou et al. [13] found that CCH is an effective hydrogen-rich agent, which can prevent liver steatosis and metabolic disorders induced by high-fat diet, by improving mitochondrial oxidative transmission, but the specific targets and mechanisms of action on the mitochondria are unclear.

In mammals, the thioredoxin (Trx) system is one of the important systems regulating the redox reactions *in vivo* [14]. The Trx system includes thioredoxin 1 (Trx1) and Trx2. Trx1 is only expressed in the cytoplasm, while Trx2 is only expressed in the mitochondria [15]. However, both of them can regulate the redox state of substrates by redox regulation and antioxidant protection [16]. Therefore, the Trx system is considered to be an important potential therapeutic target for oxidative-stress-related diseases [17]. Our previous studies have found that hydrogen can specifically upregulate cytoplasmic Trx1, which has a regulatory effect on subsequent inflammatory pathways [18], but whether hydrogen can specifically regulate mitochondrial Trx2 is not clear.

This study aimed to verify *in vivo* and *in vitro* that CCH clears excess ROS by activating mitochondrial Trx2, regulating Myo19/Drp1 activation, promoting mitochondrial peripheral division in the early stage of ARDS, protecting AT II cells, and reducing the acute lung injury of ARDS. It is important to elucidate the pathophysiological mechanism of hydrogen therapy for ARDS and to search for therapeutic targets.

2. Materials and methods

2.1. Animal experiments

Animal experiments were reviewed and approved by the Animal Care and Use Committee of Nanjing Medical University (Approval number: NMJU IACUC-2305042) and performed in strict accordance with the recommendations of the Guide for the Care and Use of Laboratory Animals (Ministry of Science and Technology of China, 2006). Pain and animal use were minimized during the experiments. Wild-type (C57 BL/6) male mice (age 6–8 weeks) and *Trx2* knockout (C57 BL/6) male mice (age 6–8 weeks) were provided by Jiangsu GemPharmatech Co., Ltd (Nanjing, China). All animals were maintained in pathogen-free conditions with a controlled temperature (22 ± 2 °C) and a standardized light/dark cycle. Animals were fed *ad libitum*. Mice were used after 7 days of adaptation. For each set of experiments, the animals were matched by age and body weight.

2.2. Experimental grouping

The *in vivo* experiment was divided into three parts. The first part determined the best treatment regimen. Fifty-five mice were randomly divided into five groups: control, lipopolysaccharide (LPS) model, LPS + H_2, LPS + CC, and LPS + CCH, to observe the 7-day survival rate and body weight changes in each group. The second part of the experiment determined the optimal time point for sampling. Ninety-nine mice were randomly divided into four large groups: control ($n = 9$), LPS ($n = 27$), LPS + CCH ($n = 27$), and CCH ($n = 9$). Mice in the LPS and LPS + CCH groups were intraperitoneally injected with LPS at 3, 6 and 12 h, with or without CCH treatment. The third part of the experiment was conducted in gene knockout mice. Nine $Trx2^{+/-}$ gene knockout mice were randomly divided into three groups: $Trx2^{+/-}$ ($n = 3$), LPS + $Trx2^{+/-}$ ($n = 3$) and LPS + CCH + $Trx2^{+/-}$ treatment ($n = 3$). Wild-type mice ($n = 3$) were used as a control, and the sampling time was 12 h after LPS treatment. Similar to the grouping for the *in vivo* experiment, the *in vitro* study was divided into four groups: control, LPS, LPS + H_2 and H_2. The cells in the different groups were collected after 3, 6 and 12 h and used for subsequent analysis.

2.3. Model preparation and treatment measures

LPS was dissolved in saline solution to a concentration of l mg/mL. The mouse model of acute lung injury in ARDS was created by a single intraperitoneal dose of 0.1 mL/10 g LPS. For the CCH treatment group, CCH suspension was prepared with drinking water on site, and administered by gavage at 50 mg/kg. Hydrogen was produced by the hydrogen cell incubator and was used for the cell experiments. Cells were cultured under an atmosphere of 60% hydrogen before treatment.

2.4. Chemicals and reagents

The hydrogen/oxygen generator (AMS-H-01) was obtained from Shanghai Asclepius Meditech Co., Ltd. (Shanghai, China). The hydrogen gas cell incubator was provided by Wuxi Gekrypton Precision Instrument Co., Ltd. (Wuxi, Jiangsu, China). Isoflurane (Webio) was purchased from Beijing Keyue Huacheng Science and Technology Co. (Beijing, China), while pentobarbital was acquired from Shanghai Yuyan Instruments Co. (Shanghai, China). Escherichia coli 055: B5 LPS was sourced from Sigma (St. Louis, MO, USA). CCH and CC were supplied by Rizhao Life Valley Biotechnology

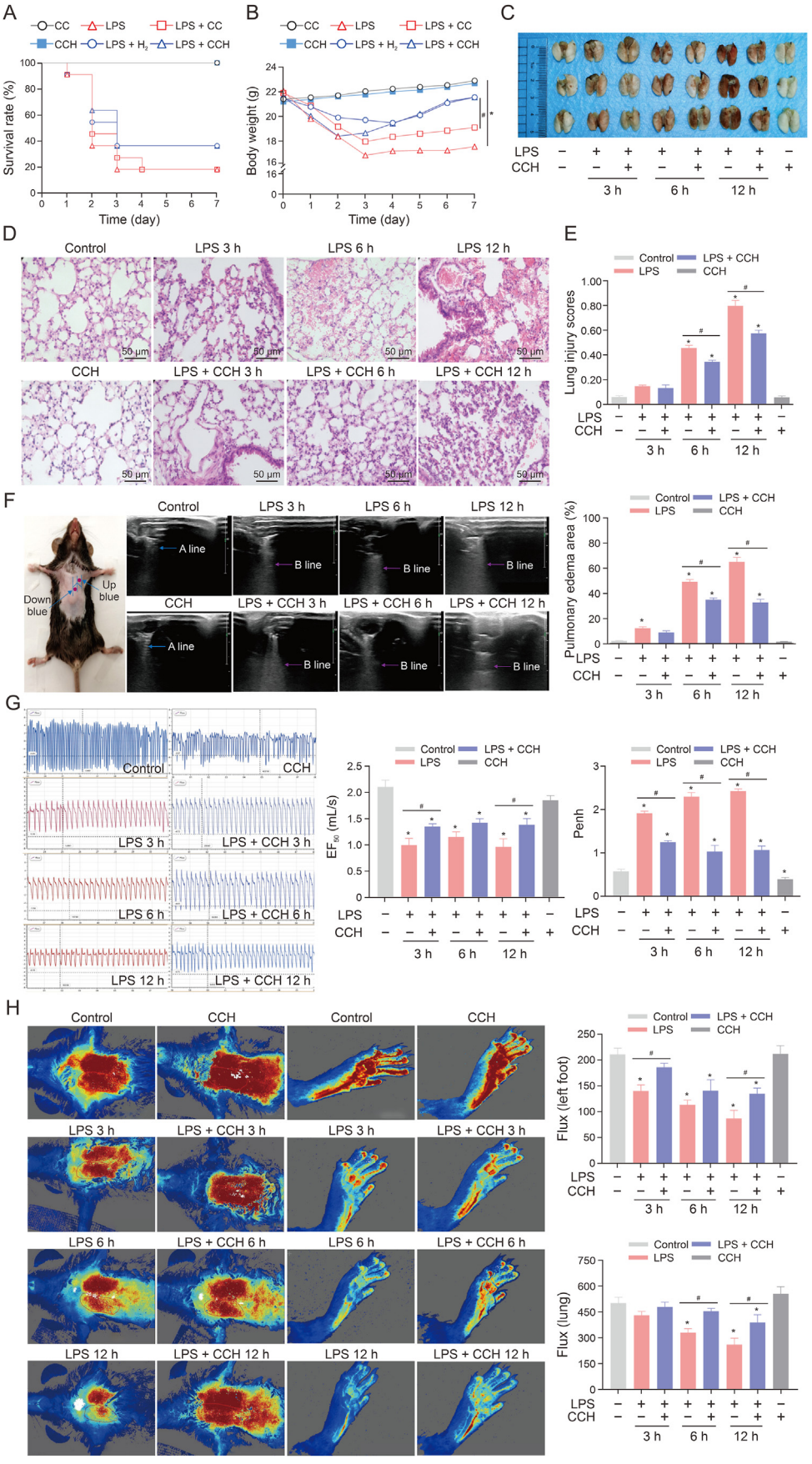
A
CC
LPS
LPS + CC
CCH
LPS + H2
LPS + CCH
Survival rate (%)
Time (day)
B
Body weight (g)
Time (day)
C
LPS
CCH
3 h
6 h
12 h
D
Control
LPS 3 h
LPS 6 h
LPS 12 h
CCH
LPS + CCH 3 h
LPS + CCH 6 h
LPS + CCH 12 h
50 μm
E
Lung injury scores
F
A line
B line
Down blue
Up blue
Pulmonary edema area (%)
G
EF50 (mL/s)
Penh
H
Flux (left foot)
Flux (lung)

Development Corporation (Rizhao, Shandong, China). Dimethylsulfoxide was obtained from Sigma (St. Louis, MO, USA). Antibodies against p-Drp1 (Ser616) (#3455, 1:1000) were purchased from Cell Signaling Technology (Beverly, MA, USA). Additional antibodies, including Trx2 (#13089-1-AP, 1:1000), COX IV (66110-1-Ig, 1:5000), Fis1 (10956-1-AP, 1:1000), and Myo19 (23906-1-AP, 1:1000), were procured from Proteintech (Chicago, IL, USA). The ROS assay kit (BL714A) was obtained from Biosharp (Hefei, China). The mitochondrial isolation kit (AKOP011) and mitochondrial membrane potential assay kit (AKOP013-1) were provided by Beijing Box Biotechnology Co., Ltd. (Beijing, China).

2.5. Cell lines

Human AT II cells (A549, ZQ0003) were purchased from the Shanghai Zhongqiao Institute of Biology (Shanghai, China). The cell lines were purchased with a STR Profiling Report.

2.6. Ultrasonic testing

Mice were anesthetized, and ultrasound testing was performed using a Philips EPIQ 5 ultrasound machine (Philips EPIQ 5, Philips Healthcare, Amsterdam, The Netherlands) and an L ultrasound probe. The scanning frequency of the probe was 3.0–12.0 MHz. Color Doppler flow imaging, pulse Doppler and serial Doppler examinations were performed while heart rate was recorded. Images with clear reflux signal and reflux spectral profiles were selected for analysis. The degree of reflux was observed, the reflux beam length and velocity were measured, and the blood flow velocity was recorded according to the appearance and duration of the reflux spectrum. The measurement method refers to the double blue point + posterolateral alveolar and/or pleural syndrome (PLAPS) point detection method to evaluate the distribution of the B line in the scanned area, which was the site of pulmonary edema, for semi-quantitative analysis [19–21]. We scanned the left and right chest, the lateral sternum to the axillary midline, the left clavicle to the upper hepatic margin, and the right clavicle to the bottom of the heart. To correct for measurement bias, a double-blind design was used during ultrasound examination. Neither the investigator nor the ultrasound operator knew the details of each group. Each mouse was examined three times. The examination was repeated by two sonographers with more than 3 years of working experience, and the average value of both measurements was taken for statistical analysis.

2.7. Lung function detector

The whole-body plethysmography (WBP) system was provided by Shanghai TOW Intelligent Technology Co., Ltd. (Shanghai, China) and was used to measure the lung function indexes in mice. Mice were placed in the testing chamber for 30 min in advance on the day of testing; the entry and conversation of unrelated personnel were reduced and the environment was quiet. Mice were placed in the tracing cavity and adapted for 10 min, and lung function parameters such as ventilation, airway obstruction and conductivity were observed.

2.8. Laser Doppler speckle flow meter

A low-power laser beam was guided to the right subclavicle of resting mice using a computer-controlled optical scanner (Moor Instruments Ltd. Millwey, Axminster, Devon, Eng.). Mice were placed on a thermostatic table, and the scanning head was placed parallel to the sole of the foot at a distance of ~20 cm. A color-coded image representing a specific relative perfusion level was displayed on the video monitor. Blood flow was recorded and measured using the moor-FLPIR-view V40 software.

2.9. Histological analysis

The perfused left lung was collected and fixed by immersion in 4% paraformaldehyde for 24 h, dehydrated in 70%, 80%, 90%, 95% and 100% alcohol, and cut into xylene-transparent, paraffin-embedded, 5-μm sections, and the degree of lung injury was scored after hematoxylin and eosin (HE) staining. The lung injury scoring standard was based on the American Thoracic Society (ATS) pathology scoring system for acute lung injury (Table S1) [22]. Target proteins were evaluated using immunohistochemistry and immunofluorescence.

2.10. Mitochondrial isolation

Lung tissue (0.1 g) or 5 million cells were collected and ground on ice, and the supernatant was removed by centrifugation at 600 *g* for 5 min at 4 °C. Mitochondria were isolated using the Mitochondrial Isolation and Enzyme Extraction Kit (boxbio; Beijing Box Production Technology Co. Ltd., Beijing, China). The isolated mitochondria were collected and used for subsequent experiments.

2.11. Western blotting

Lung tissue and serum samples were lysed with radioimmunoprecipitation assay (RIPA) lysis buffer containing phosphatase protease inhibitors and phenylmethylsulfonyl fluoride, while cell samples were lysed with immunoprecipitation (IP) cell lysis buffer. The bicinchoninic acid assay (BCA) method was used to quantify the total protein concentration. 10% sodium dodecyl sulfate polyacrylamide gel electrophoresis (10% SDS-PAGE) was prepared for detection of tissue factor (TF) and β-actin, and 15% SDS-PAGE was prepared for detection of Trx2. Protein samples (10 μL/lane) were separated by 12% SDS-PAGE, and blocked by 5% skimmed milk for 1 h at room temperature, and primary antibody was added overnight at 4 °C. After Tris-buffered saline with Tween 20 (TBST) rinsing, the cells were incubated with horseradish-peroxidase-labeled secondary antibody for 2 h at room temperature. The results were analyzed after 1 min of color development of the enhanced chemiluminescence (ECL) luminescent substrate.

2.12. Transmission electron microscopy

The lungs were excised from the mice and immediately immersed in 4% paraformaldehyde and fixed for 24 h. The fixed lung samples were embedded in paraffin wax and sliced into 4-μm

Fig. 1. Coral calcium hydrogenation (CCH) significantly alleviated lipopolysaccharide (LPS)-induced acute respiratory distress syndrome (ARDS) acute lung injury. (A) The survival rate was observed for 7 days ($n = 11$ in each group). LPS (10 mg/kg, i.p.) was used to establish ARDS mice. Mice were treated with CCH (50 mg/kg, i.g.). (B) Weight change of mice were measured daily for 7 consecutive days ($n = 11$ in each group). (C) Representative images of lung tissues after LPS injection at different time points ($n = 3$ in each group). (D) Hematoxylin and eosin (HE) staining was used to observe the lung histopathological change ($n = 3$ in each group). (E) Lung injury score was used to evaluate the lung histopathological injury ($n = 3$ in each group). (F) Representative images of B-mode ultrasound from lungs of mice in different groups ($n = 5$ in each group), with arrows indicating B lines. (G) Lung function curves were observed by whole-body plethysmography in mice from different groups at 3, 6 and 12 h ($n = 5$ in each group). (H) Representative lung (left) and left hind foot (right) images and changes in blood flow in mice in different groups ($n = 5$ in each group). Data are presented as means ± standard deviation (SD) and were analyzed by one-way analysis of variance (ANOVA) followed by Bonferroni's post hoc test. $^{*}P < 0.05$ versus control; $^{\#}P < 0.05$ versus LPS-induced group.

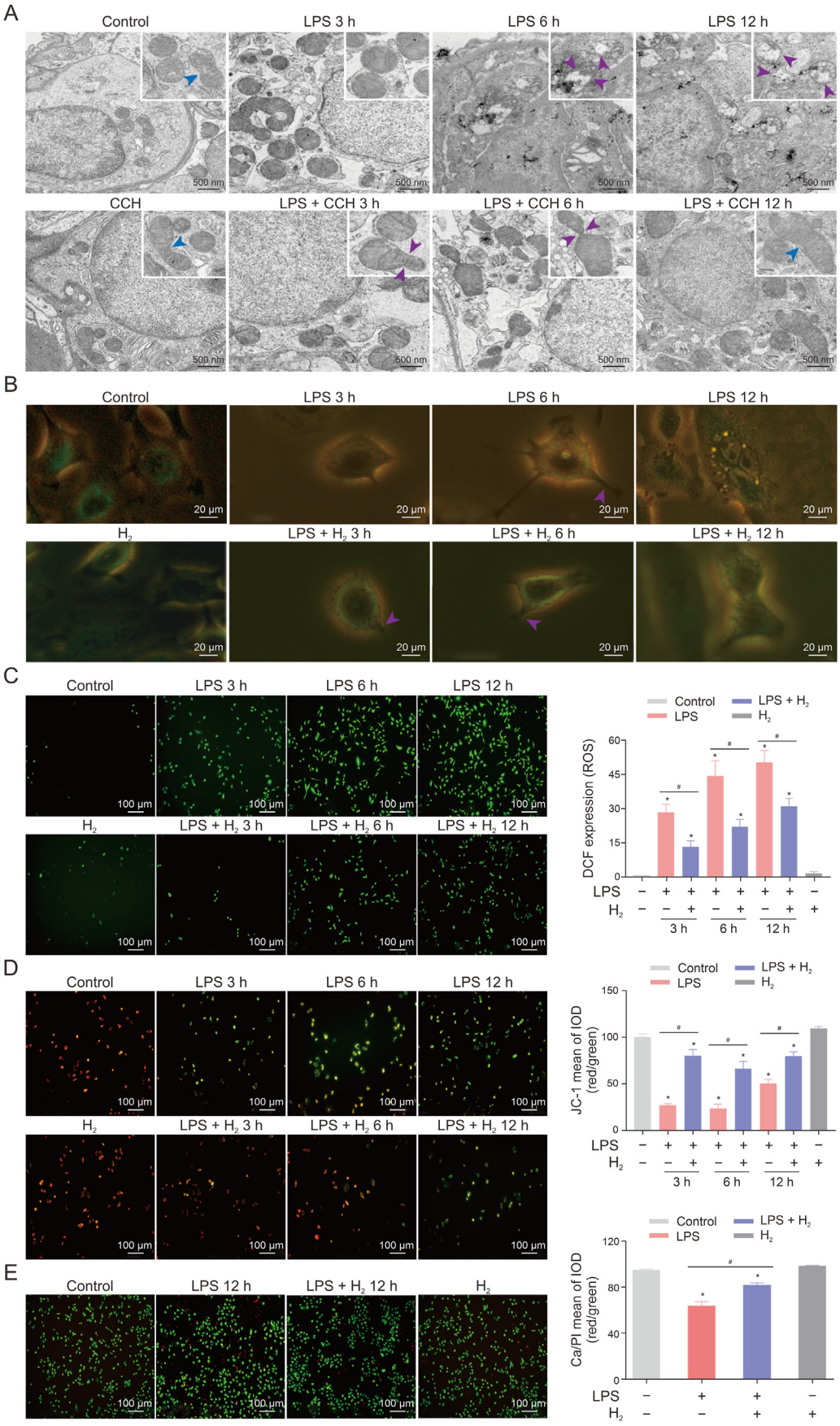
A
Control
LPS 3 h
LPS 6 h
LPS 12 h
CCH
LPS + CCH 3 h
LPS + CCH 6 h
LPS + CCH 12 h
500 nm
B
Control
LPS 3 h
LPS 6 h
LPS 12 h
H2
LPS + H2 3 h
LPS + H2 6 h
LPS + H2 12 h
20 μm
C
100 μm
Control
LPS
LPS + H2
H2
DCF expression (ROS)
3 h
6 h
12 h
D
JC-1 mean of IOD (red/green)
E
Ca/PI mean of IOD (red/green)

thick sections. Ultrathin sections were cut and double stained with uranyl acetate and lead citrate. Mitochondrial morphology was observed by transmission electron microscopy.

2.13. Quantitative real-time polymerase chain reaction (qRT-PCR)

Mouse alveolar lavage fluid was collected. RNA was extracted with TRIzol reagent (Invitrogen, Carlsbad, CA, USA) and the concentration was determined. For qRT-PCR detection, A549 cells were seeded in six-well plates. The selected primer sequences for *Trx2* were designed as follows: forward primer CTGGTGGCCTGACTGTAACAC and reverse primer TGACCACTCGGTCTTGAAAGT. After different treatments, total cell RNA was extracted using TRIzol reagent. Reverse transcription of RNA was performed by Hiscript III RT SuperMix for qPCR (+gDNA wiper) (Vazyme, Nanjing, China), which was subjected to ChamQ SYBR qPCR Master Mix (High ROX Premixed) and the Applied Biosystems StepOne system (Vazyme, Nanjing, China). Cytokine mRNA levels were normalized to the housekeeping gene, *glyceraldehyde-3-phosphate dehydrogenase* (*GAPDH*), with the $2^{-\Delta\Delta Ct}$ method.

2.14. Plasmid and siRNA transfection

The National Center for Biotechnology Information GenBank sequence database was accessed, and the BLAST tool was used to identify the human expressed sequence tag (EST)-encoded protein homologous to murine *Trx2*. Multiple EST sequences were aligned to murine *Trx2*, and contiguous sequences were deduced by merging with overlapping EST. A549 cells were plated at a density of 100,000 per well in six-well plates. High-quality *Trx2* overexpression plasmid, *Trx2* siRNA and the corresponding PolyPlus jetPRIME transfection reagent constructed by Shanghai Hanheng Biotechnology Co., Ltd. (Shanghai, China) were added to each well and placed in an incubator under an atmosphere of 95% air and 5% CO_2 for transfection. Transfection efficiency and cell status were observed daily by fluorescence microscopy, and the transfected A549 cells were harvested 48−72 h later. Transfection efficiency was evaluated by Western blotting and qRT-PCR. Validated *Trx2*-overexpressing (OE) cells were used for subsequent experiments.

2.15. Statistical analysis

All statistical analyses were performed using GraphPad Prism version 6. The numerical data were fitted to a normal distribution, and continuous variables were expressed as mean ± standard deviation (SD). Changes in control distribution of protein expression and changes in behavioral response were detected by Student's *t*-test and univariate analysis of variance (ANOVA). Differences in latency over time between groups were tested by two-way ANOVA. The Bonferroni post hoc test was used for comparisons between multiple groups. $P < 0.05$ was considered statistically significant.

3. Results

3.1. CCH can attenuate lung injury in mice with LPS-induced ARDS

Mice were injected intraperitoneally with LPS, and the effects of CCH administration and 4% hydrogen inhalation were observed. The 7-day survival rate showed that the CCH and hydrogen treatment groups had a significantly higher survival rate than the LPS group, However, there was no significant difference between CCH and hydrogen treatment groups (Fig. 1A). Body weight of the mice was continuously observed over 7 days. The weight changes in the CCH- and hydrogen-treated mice were similar. The downward trend was significantly slower compared with the LPS and LPS + CC groups (Fig. 1B). CCH, similar to hydrogen, was protective in LPS-induced ARDS mice, and the mechanism by which CCH acted was largely dependent on released hydrogen instead of carrier CC. To reduce animal use, subsequent experiments were performed using the control, LPS model, LPS + CCH treatment, and CCH treatment groups. Observation of lung tissue and HE staining of sections revealed red blood cell leakage and neutrophil infiltration in the alveolar space of LPS mice, which gradually increased with time. The red blood cell leakage and neutrophil infiltration in LPS + CCH group were significantly reduced compared with that in the LPS group at the same time point (Figs. 1C and D). Lung injury pathology scores showed a significant decrease at 6 and 12 h in the LPS + CCH treatment group (Fig. 1E). Ultrasound showed that the extent of lung edema in the LPS + CCH-treated group was significantly reduced compared with that in the LPS mice at the same time point (Fig. 1F). Lung function testing revealed significantly improved lung airway compliance in the LPS + CCH-treated mice compared with the LPS group (Fig. 1G). Speckle Doppler flowmetry showed that pulmonary blood flow velocity in LPS mice after 3 h decreased progressively with time, and local microcirculation blood flow velocity significantly improved after CCH treatment (Fig. 1H).

3.2. The regulation of early mitochondrial fission by CCH

Lung tissues from mice were collected for transmission electron microscopy. We found that mitochondria in lung tissues of ARDS mice were morphologically altered at 3 h, with mitochondrial swelling and breakage of the cristae structure. Vacuoles were present in the mitochondria at 6 h with faintly visible nonvacuolar cristae, and were concentrated at the sides of the mitochondria. Peripheral division of mitochondria was obvious (Fig. 2A, red arrow). By 12 h, vacuoles further expanded, with residual cristae aggregation and complete vacuolated mitochondria splitting. In the CCH treatment group, peripheral division was prominent at 3 and 6 h, while normal central division was observed at 12 h (Fig. 2A, blue arrow). Mitochondrial fluorescent probe staining of live A549 cells revealed that LPS-treated A549 alveolar epithelial cells appeared enriched with spherical mitochondria at 3 h. Labeled mitochondrial fragments containing fluorescent markers were observed separating from the mitochondrial rim in the hydrogen-treated group of cells (Fig. 2B, red arrow). Immunofluorescence detected ROS release from A459 cells, and found that the ROS content increased gradually in the LPS group, but decreased significantly in the hydrogen-treated and LPS groups (Fig. 2C). Mitochondrial membrane potential was observed by immunofluorescence; the control potential showed red fluorescence, and the proportion of cells with green fluorescence increased for 3 h. This indicated that the decrease in mitochondrial membrane potential became more obvious with time, and was inhibited after hydrogen treatment (Fig. 2D). Calcein/propidium iodide (PI) staining was used to observe the cell viability after 12 h of modeling, and the cell viability of the hydrogen

Fig. 2. Hydrogen promotes early mitochondrial peripheral division and stabilizes mitochondrial function. (A) Lung tissue cryo-scanning electron microscopy showed the trend in peripheral division after coral calcium hydrogenation (CCH) therapy ($n = 3$ in each group). (B) A549 living cell mitochondrial tracer fluorescence staining showed the trend in peripheral division after hydrogen therapy ($n = 3$ in each group). (C) Representative images of immunofluorescence staining for reactive oxygen species (ROS) ($n = 3$ in each group). (D) Representative images of immunofluorescence staining for mitochondrial membrane potential ($n = 3$ in each group). (E) Calcein/propidium iodide (PI) staining was performed to detect viability ($n = 3$ in each group). Data are presented as means ± standard deviation (SD), and were analyzed by one-way analysis of variance (ANOVA) followed by Bonferroni's post hoc test. *$P < 0.05$ versus Control; #$P < 0.05$ versus lipopolysaccharide (LPS)-induced group. DCF: dichlorofluorescein; IOD: integrated optical density.

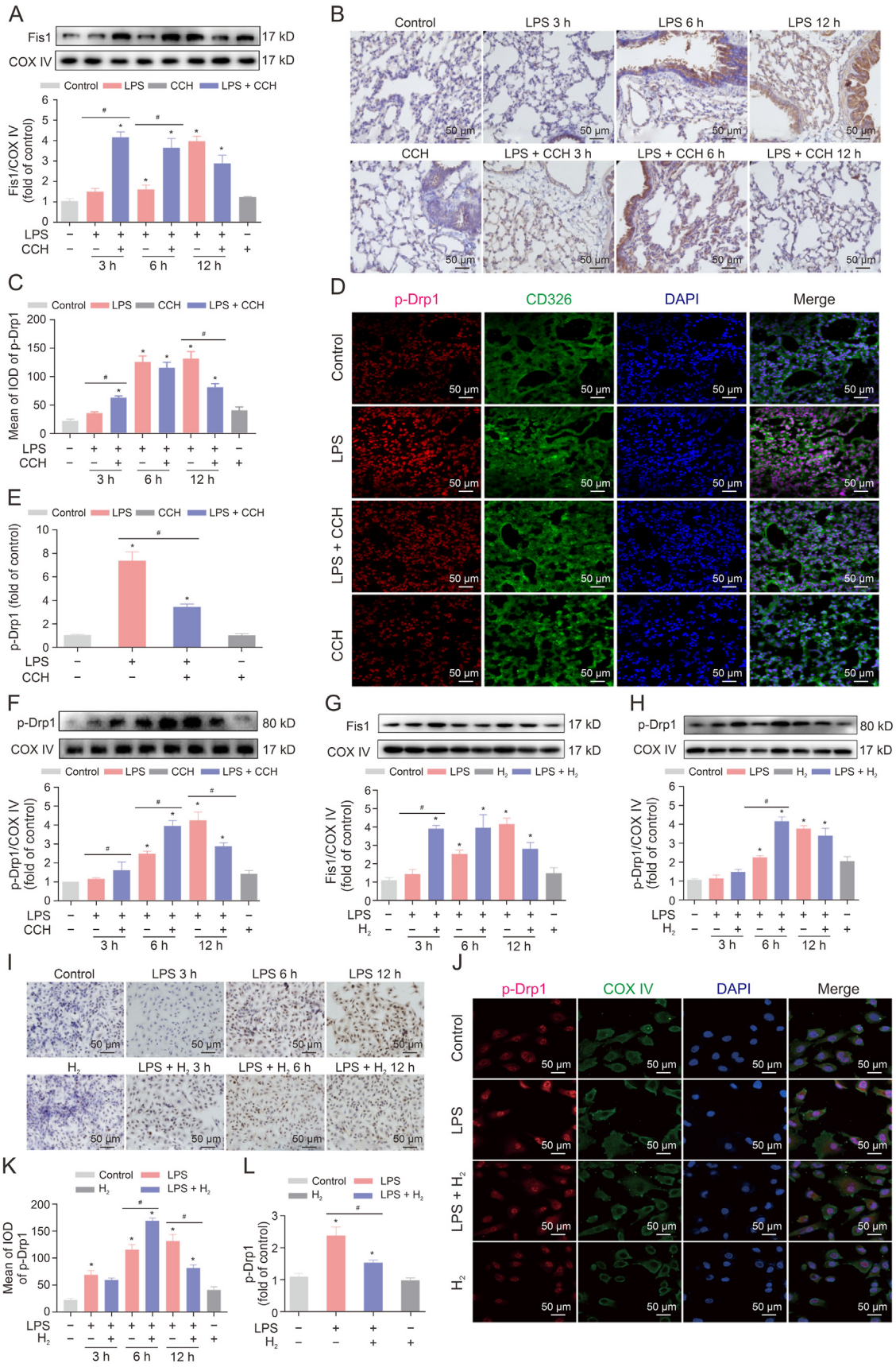

Fig. 3. Coral calcium hydrogenation (CCH) regulates the activation of p-dynamin-related protein 1 (Drp1) to promote mitochondrial peripheral division. (A) Representative images of Western blot for Fis1 protein ($n = 3$ in each group). (B) Representative images of immunohistochemical staining ($n = 3$ in each group). (C) Quantitative immunohistochemical analysis of p-Drp1 in lung tissue ($n = 3$ in each group). (D) Representative images of immunofluorescence staining ($n = 3$ in each group) of lung tissue. (E) Quantitative analysis of optical density value of p-Drp1 immunofluorescence in lung tissue at 12 h ($n = 3$ in each group). (F) Representative images of Western blot for p-Drp1 protein ($n = 3$ in each group).

treatment group was significantly better than that of the modeling group (Fig. 2E).

3.3. CCH regulates the activation of mitochondrial fission proteins Fis1/p-Drp1

CCH regulates the activation of p-Drp1, a key protein of mitochondrial fission, to promote mitochondrial peripheral division. Mitochondria were purified from lung tissue Western blotting of Fis1 (Fig. 3A), immunohistochemical staining (Figs. 3B and C),12-h lung sections of immunofluorescence staining (Figs. 3D and E) and Western blotting of p-Drp1 (Fig. 3F) showed that the activation trend of Fis1/p-Drp1 in the LPS-induced group was progressively increased. While the expression of p-Drp1 in the CCH treatment group was significantly lower than that in the LPS model group. Mitochondria of A549 cells were isolated and expression of Fis1/p-Drp1 and Fis 1 were detected by Western blotting. Western blotting showed that p-Drp1 and Fis1 in the hydrogen treatment group was significantly increased at 3 h and decreased at 12 h (Figs. 3G and H). Immunohistochemical (Fig. 3I) and immunofluorescence (Fig. 3J) of A549 cells results showed that the activation trend of p-Drp1 in the LPS group was progressively increased (Fig. 3K), while in the hydrogen treatment group, p-Drp1 expression in A549 cells significantly lower than that in the LPS group at 12 h (Fig. 3L).

3.4. CCH activates Trx2 to regulate the activation of Myo19/p-Drp1, maintaining mitochondrial fission

Molecular hydrogen mediates the activation of Myo19, another key protein of peripheral division. Immunohistochemical staining was used to observe the expression of Myo19 in lung tissue (Fig. 4A). Myo19 showed high expression at 3 h after hydrogen intervention and continued at 12 h (Fig. 4B). Mitochondria were purified from lung tissue. Western blotting showed that the activation trend of Myo19 was progressively increased in the CCH treatment group (Fig. 4C). Immunofluorescence of lung tissue showed that the activation of Myo19 in the CCH group was significantly increased than that in the LPS group at 12 h (Fig. 4D). Immunohistochemical staining was used to observe the expression of Myo19 in A549 cells (Fig. 4E). Myo19 showed high expression at 3 h after hydrogen intervention and continued at 12 h (Fig. 4F). Western blotting showed the activation of Myo19 in the hydrogen treatment group was significantly increased than that in the LPS group at 3 and 6 h (Fig. 4G). Immunofluorescence of A549 cells showed that the activation of Myo19 in the hydrogen treatment group was significantly increased than that in the LPS group at 12 h (Fig. 4H).

We further investigated that molecular hydrogen mediates the activation of Trx2, a key protein of oxidative stress. Immunohistochemical staining was used to observe the expression of Trx2 in lung tissue of mice (Fig. 5A). Trx2 showed high expression at 3 h after hydrogen intervention and continued at 6 h and 12 h (Fig. 5B). Mitochondria were purified from lung tissue. Western blotting showed that the activation trend of Trx2 was progressively increased in the CCH treatment group (Fig. 5C). Immunofluorescence of lung tissue showed that the activation of Trx2 in the CCH group was significantly increased than that in the LPS group at 12 h (Fig. 5D). Immunohistochemical staining was used to observe the expression of Trx2 in A549 cells (Fig. 5E). Trx2 showed high expression at 3 h after hydrogen intervention and continued at 6 and 12 h (Fig. 5F). Western blotting showed the activation of Trx2 in the hydrogen treatment group was significantly increased than that in the LPS group at 3 and 6 h (Fig. 5G). Immunofluorescence of A549 cells showed that the activation of Trx2 in the hydrogen treatment group was significantly increased than that in the LPS group at 12 h (Fig. 5H).

The protective effect of CCH against lung injury in ARDS mice was observed using $Trx2^{+/-}$ knockout mice. Ultrasonic examination of the lung (Fig. 6A) showed that the $Trx2^{+/-}$ mice had pulmonary edema; the severity of which was close to that of the LPS-induced ARDS mice at 12 h, and the severity did not decrease in $Trx2^{+/-}$ ARDS mice after CCH treatment. Lung function test (Fig. 6B) showed that the lung respiratory resistance of $Trx2^{+/-}$ mice was significantly increased compared with that of normal mice, and the lung respiratory resistance of CCH treated $Trx2^{+/-}$ ARDS mice was not improved compared with ARDS mice. Speckle Doppler detection of local pulmonary blood flow (Fig. 6C) showed that the pulmonary circulation velocity of $Trx2^{+/-}$ mice was significantly slower than that of normal group, and CCH treatment of $Trx2^{+/-}$ ARDS mice did not accelerate the pulmonary blood flow velocity compared with ARDS mice. HE section (Fig. 6D) of lung tissue showed that compared with the control group, $Trx2^{+/-}$ mice had high neutrophil infiltration in the lung interstitium, thickened septa hyaline, and a small amount of red blood cell leakage. The extent of injury was similar to that in ARDS mice induced by LPS for 12 h, whereas lung injury in $Trx2^{+/-}$ knockout ARDS mice did not improve after CCH treatment. Lung tissues from mice at 12 h after LPS treatment were removed for mitochondrial purification. Western blotting confirmed that Trx2 suppression was obvious in $Trx2^{+/-}$ knockout mice compared with mice in the normal group. Trx2, Myo19 and p-Drp1 expressions were significantly decreased in $Trx2^{+/-}$ knockout mice compared with those in the LPS modeling group, whereas no significant upward trend of the above proteins was detected after CCH treatment (Fig. 6E). The above results suggest that *Trx2* knockout abolished the protective effect of CCH in ARDS mice and is more susceptible to LPS-induced lung injury in ARDS.

We used plasmid transfection to overexpress *Trx2* and siRNA to knock down *Trx2* in A549 cells. qPCR confirmed plasmid transfection with overexpression of *Trx2* (Fig. 7A) and siRNA silencing *Trx2* (Fig. 7B) in A549 cells. Western blotting also confirmed plasmid transfection with overexpression of Trx2 (Fig. 7C) and siRNA silencing Trx2 (Fig. 7D) in A549 cells. LPS-induced A549 cells overexpressing Trx2 for 12 h were extracted, and western blotting was performed after mitochondrial purification. Compared with the LPS-induced group, cells with overexpression of Trx2 and hydrogen-treated cells had up-regulated Myo19 and down-regulated P-Drp1 expression (Fig. 7E). Expression of Myo19 in the Trx2 plus LPS group was significantly lower than in the LPS model group, and expression of p-Drp1 was significantly higher (Fig. 7F). This suggests that expression of Trx2 is closely related to expression of Myo19 and p-Drp1 (Fig. 7G).

4. Discussion

The main findings of this study were as follows. (1) Continuous release of hydrogen in the body through CCH treatment was effective for treatment of acute lung injury in ARDS. (2) Early activation of Trx2 enhanced activation of key proteins involved in mitochondrial peripheral division, namely Myo19 and Fis/P-Drp1,

(G) Representative Western blot images of Fis1 ($n = 3$ in each group). (H) Representative Western blot images of p-Drp1 ($n = 3$ in each group). (I) Representative images of immunohistochemical staining of A549 cells. ($n = 3$ in each group) (J) Representative images of immunofluorescence staining of A549 cells ($n = 3$ in each group). (K) The plot of integral optical density (IOD) of p-Drp1 in A549 cell mitochondria ($n = 3$ in each group). (L) The plot of mean fluorescence intensity of p-Drp1 ($n = 3$ in each group). Data are presented as means ± standard deviation (SD), and were analyzed by one-way analysis of variance (ANOVA) followed by Bonferroni's post hoc test. $^{*}P < 0.05$ versus control; $^{\#}P < 0.05$ versus LPS-induced group. DAPI: 4',6-diamidino-2-phenylindole.

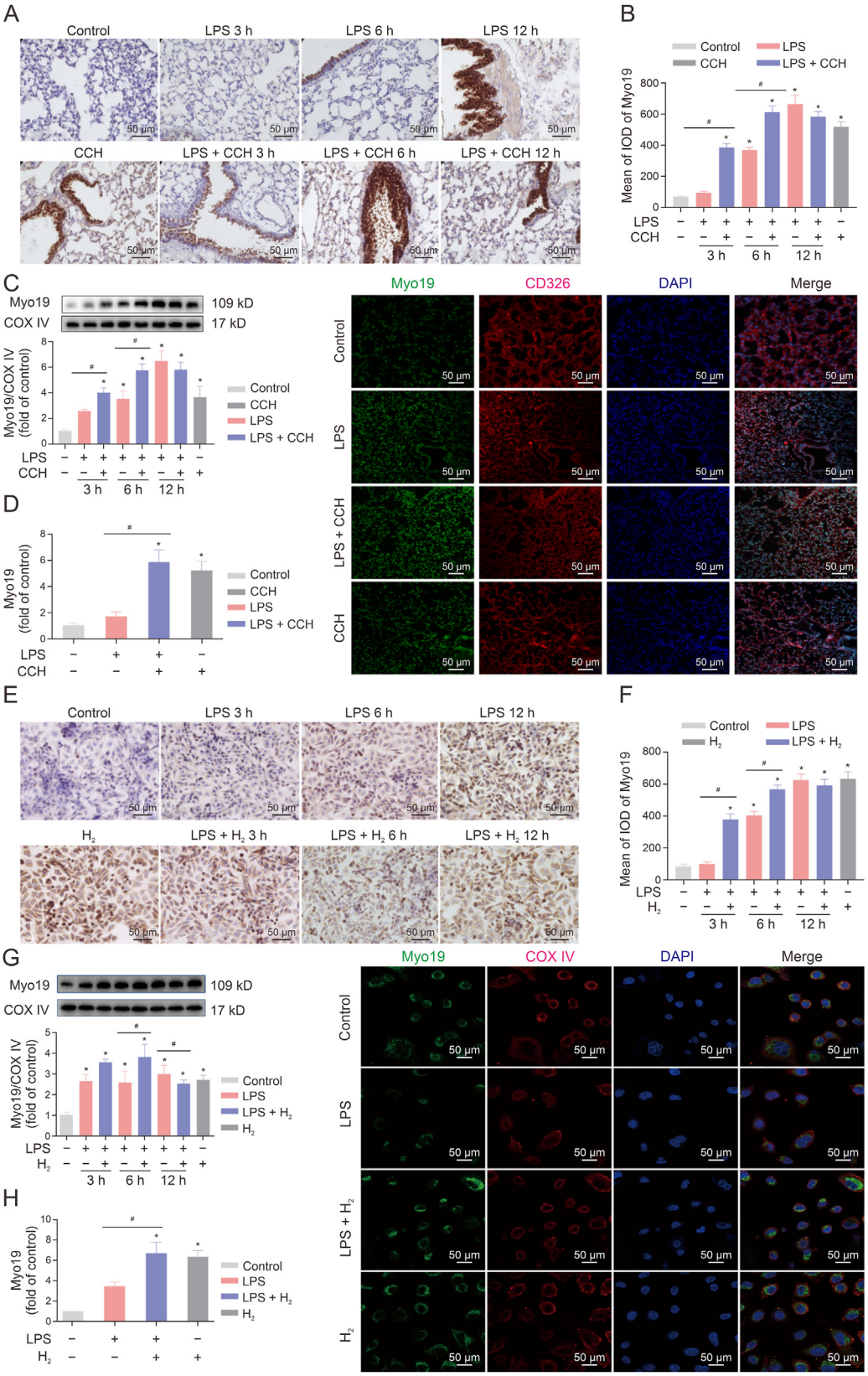

Fig. 4. Molecular hydrogen mediates the activation of Myo19. (A) Representative images of immunohistochemical staining for Myo19 in lung tissue ($n = 3$ in each group). (B) The plot of integral optical density (IOD) of Myo19 in lung tissue ($n = 3$ in each group). (C) Mitochondria were purified from lung tissue. Representative images of Western blot for Myo19 ($n = 3$ in each group) and quantitative analysis. (D) The plot of mean fluorescence intensity of Myo19 and representative images of immunofluorescence staining for Myo19 in lung sections removed at 12 h ($n = 3$ in each group). (E) Representative images of immunohistochemical staining for Myo19 in A549 cells ($n = 3$ in each group). (F) The plot of IOD of Myo19 in A549 cells ($n = 3$ in each group). (G) A549 cell mitochondria were purified. Representative images of Western blot for Myo19 ($n = 3$ in each group). (H)The plot of mean fluorescence intensity of Myo19 and representative images of immunofluorescence staining for Myo19 in A549 cells at 12 h ($n = 3$ in each group). Data are presented as means ± standard deviation (SD), and were analyzed by one-way analysis of variance (ANOVA) followed by Bonferroni's post hoc test.$^{*}P < 0.05$ versus control; $^{\#}P < 0.05$ versus lipopolysaccharide (LPS)-induced group. DAPI: 4',6-diamidino-2-phenylindole.

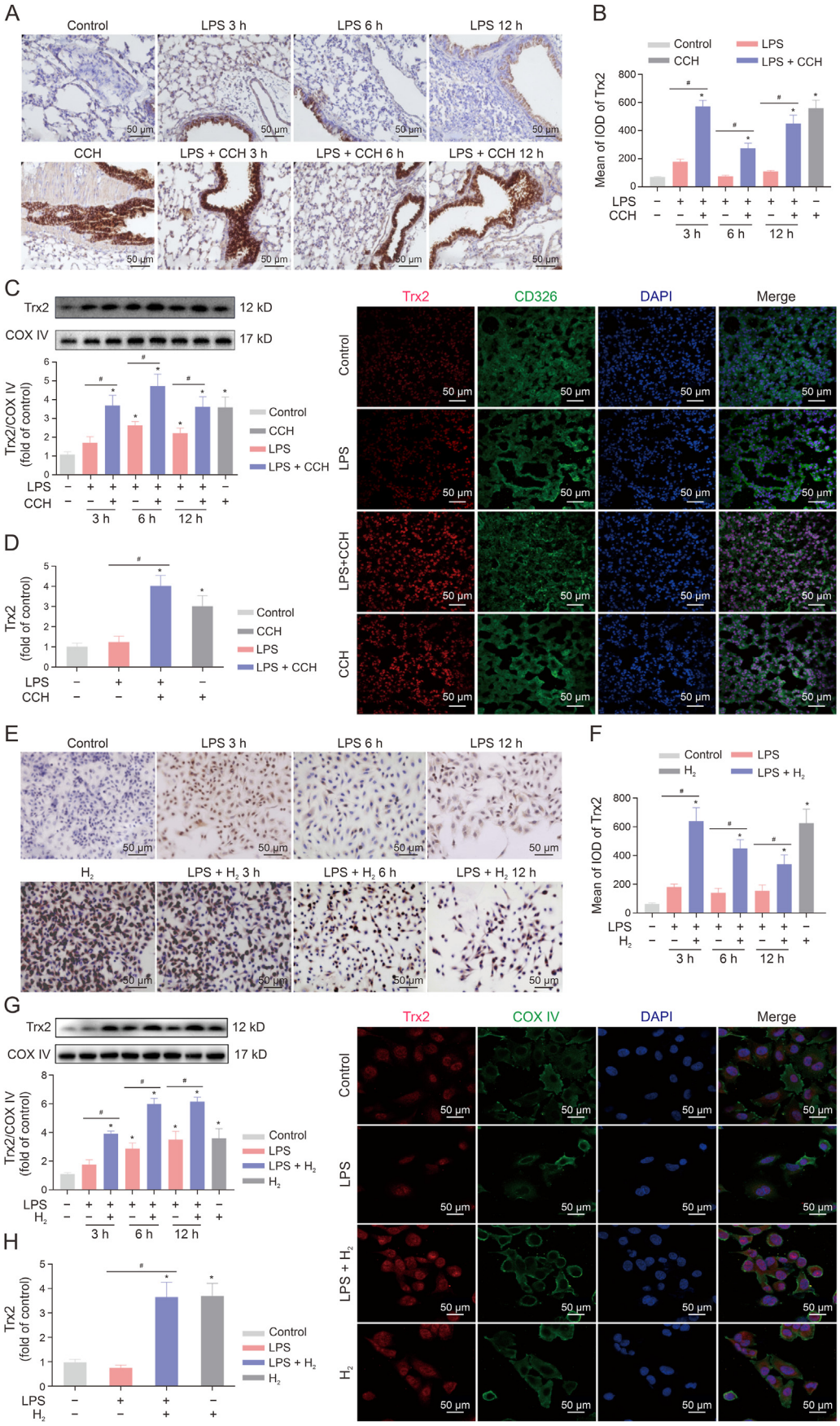

Fig. 5. Molecular hydrogen mediates the activation of Trx2. (A) Representative images of immunohistochemical staining for Trx2 in lung tissue ($n = 3$ in each group). (B) The plot of integral optical density (IOD) of Trx2 in lung tissue ($n = 3$ in each group). (C) Mitochondria were purified from lung tissue. Representative images of Western blot for Trx2 ($n = 3$ in each group) and quantitative analysis. (D) The plot of mean fluorescence intensity of Trx2 and representative images of immunofluorescence staining for Trx2 in lung sections

during the early stage of ARDS. This promoted early local clearance of mitochondria and maintained a healthy balance within lung mitochondria. Conversely, knockout of the *Trx2* gene exacerbated acute lung injury in ARDS. (3) CCH upregulated expression of Trx2, thereby maintaining mitochondrial quality control and improving acute lung injury associated with ARDS. (4) Through the Trx2/Myo19/P-Drp1 signaling pathway, hydrogen maintained mitochondrial functional balance in AT II cells and alleviated oxidative stress damage caused by ROS.

Hydrogen is a colorless, odorless, and nontoxic gas that selectively neutralizes oxygen free radicals, thereby exerting antioxidative and anti-inflammatory effects. Ohsawa et al. [23] discovered that 2% hydrogen improved cerebral ischemia and hypoxia in rats. In our previous study, we found that inhalation of 4% hydrogen specifically activated Trx1, leading to improvements in pulmonary microcirculation and reduction in inflammation in ARDS mice [24]. Despite its therapeutic efficacy for ARDS lung injury, the flammable and explosive nature of hydrogen hinders its application. Therefore, the development of safe and effective hydrogen carrier preparations remains an important focus in medical research. The porous powder CCH is synthesized through the reaction of CC and hydrogen at high temperatures and pressures ranging from 800 to 950 °C. It serves as a novel solid carrier for negative hydrogen ions, capable of instantaneously generating hydrogen upon contact with water [25]. Suspensions containing 5–10 g/L CCH can achieve a maximum concentration of hydrogen up to 600 ppb, with sustained release lasting for at least 24 h [26]. While CCH has exhibited promising antioxidative stress effects in cerebral ischemia reperfusion and liver metabolism, its potential protective role in ARDS-induced lung injury remains unclear. In this study, we observed that oral administration of CCH significantly improved acute lung injury in ARDS mice. Furthermore, CCH treatment alleviated acute pulmonary edema and pulmonary hemorrhage, reduced pulmonary respiratory resistance, and enhanced local microcirculation in mice. By evaluating the 7-day survival rate and weight change, the therapeutic effect of oral CCH in mice was consistent with that of inhaled hydrogen, strongly suggesting similarity between the therapeutic effects of oral CCH and inhaled hydrogen. CC primarily consists of calcium carbonate and shares a close composition resemblance to human bone. Our findings revealed a significant difference in the survival rate among ARDS mice treated with oral CCH versus CC alone. The treatment outcome for mice receiving oral CC resembled that of untreated ARDS mice, resulting in a significantly higher mortality rate compared with those receiving CCH or hydrogen inhalation therapy. This confirms that the beneficial effects CCH on ARDS are mainly attributed to hydrogen release rather than CC itself.

AT II cells play a crucial role in the occurrence and progression of ARDS [27,28]. Mitochondrial dysfunction resulting from an imbalance in ROS is a significant factor contributing to AT II cell damage and ultimately leading to ARDS [29,30]. Lian et al. [31]demonstrated that hydrogen inhibited total Drp1 expression in mitochondria of human umbilical vein endothelial cells induced by LPS through the heme oxygenase-1 pathway. This maintained mitochondrial homeostasis via the PINK1/Parkin mitochondrial autophagy pathway, suggesting that hydrogen targets mitochondria as important mediators for exerting biological effects. Previous studies have found that CCH, as a highly efficient hydrogen-rich agent, enhanced mitochondrial function by activating phase II enzymes in the mitochondrial respiratory chain to prevent liver steatosis in obese rats induced by high-fat diet. Thus, CCH is considered to possess potential as a mitochondrial nutrient. In the present study, we observed that the pulmonary mitochondria of ARDS mice exhibited a pronounced tendency towards extensive vacuolation and fragmentation at 12h. However, following CCH treatment, the morphology of pulmonary mitochondria in ARDS mice significantly improved, with a notable reduction in abnormal division. Additionally, mitochondrial staining of living A549 cells *in vitro* revealed that after 12h LPS induction, the cells displayed evident vacuole-like structures and enriched mitochondrial components. Conversely, the hydrogen treatment group showed control cell division morphology and more evenly distributed mitochondria around the nuclei. Assessment of cellular ROS content and mitochondrial membrane potential confirmed a significant decrease in ROS levels in A549 cells after hydrogen treatment. The declining trend in mitochondrial membrane potential was significantly inhibited. These findings strongly suggest that hydrogen released from CCH improves oxidative stress damage associated with ARDS by preserving stable mitochondrial function within alveolar epithelial cells. What mechanism underlies the ability of hydrogen to maintain mitochondrial function stability?

Mitochondria are highly dynamic organelles, and their morphology, quantity, and size are regulated by the mitochondrial quality control system through processes of division and fusion to maintain control function. In ARDS, oxidative stress leads to the release of mitochondrial ROS and other free radicals, disrupting the balance of the mitochondrial dynamic network and exacerbating inflammatory lung injury. Studies have shown that during the early stage of the mitochondrial antioxidative stress response, division plays a predominant role [32]. By morphological characteristics and outcomes of division events, previous studies have discovered two forms of mitochondrial division: (1) symmetrical division from the central region as a behavior associated with control proliferation; and (2) peripheral division starting from one side after oxidative stress stimulation, which is closely linked to clearance of harmful substances from the mitochondria. Both types rely on Drp1 mediation, while Fis1 ligand significantly influences peripheral division. In this study, we observed that expression of Fis1 protein in the lungs of ARDS mice significantly increased within 3 h after CCH treatment, and a similar trend was observed for P-Drp1. However, upregulation of Fis1/P-Drp1 in the ARDS mice was delayed. The trend of Fis1/P-Drp1 *in vitro* closely mirrored that observed *in vivo*, suggesting that CCH initiated a partial clearance mechanism in early lung mitochondria during ARDS. Further studies found that when the body was stimulated by oxidative stress, mitochondria could recognize and migrate damaged mtDNA expressed on the mitochondrial side through a series of unknown mechanisms, and then divide the damaged from the normal mitochondria through fission to avoid further damage [33]. In this study, we observed in frozen sections of lung tissues significant mitochondrial peripheral division in CCH-treated ARDS mice at 3 h, whereas the mitochondria in the lungs of the ARDS model mice appeared to be globularly swollen at 3 h, and significant mitochondrial peripheral division appeared at 6 h, suggesting that the time of mitochondrial peripheral division was advanced by CCH treatment. Immunofluorescence of live cells confirmed the above trend in peripheral division. The mechanism of

removed at 12 h ($n = 3$ in each group). (E) Representative images of immunohistochemical staining for Trx2 in A549 cells ($n = 3$ in each group). (F) The plot of IOD of Trx2 in A549 cells ($n = 3$ in each group). (G) A549 cell mitochondria were purified. Representative images of Western blot for Trx2 ($n = 3$ in each group). (H) The plot of mean fluorescence intensity of Trx2 and representative images of immunofluorescence staining for Trx2 in A549 cells at 12 h ($n = 3$ in each group). Data are presented as means ± standard deviation (SD), and were analyzed by one-way analysis of variance (ANOVA) followed by Bonferroni's post hoc test. $^{*}P < 0.05$ versus control; $^{\#}P < 0.05$ versus lipopolysaccharide (LPS)-induced group. CCH: coral calcium hydrogenation; DAPI: 4',6-diamidino-2-phenylindole.

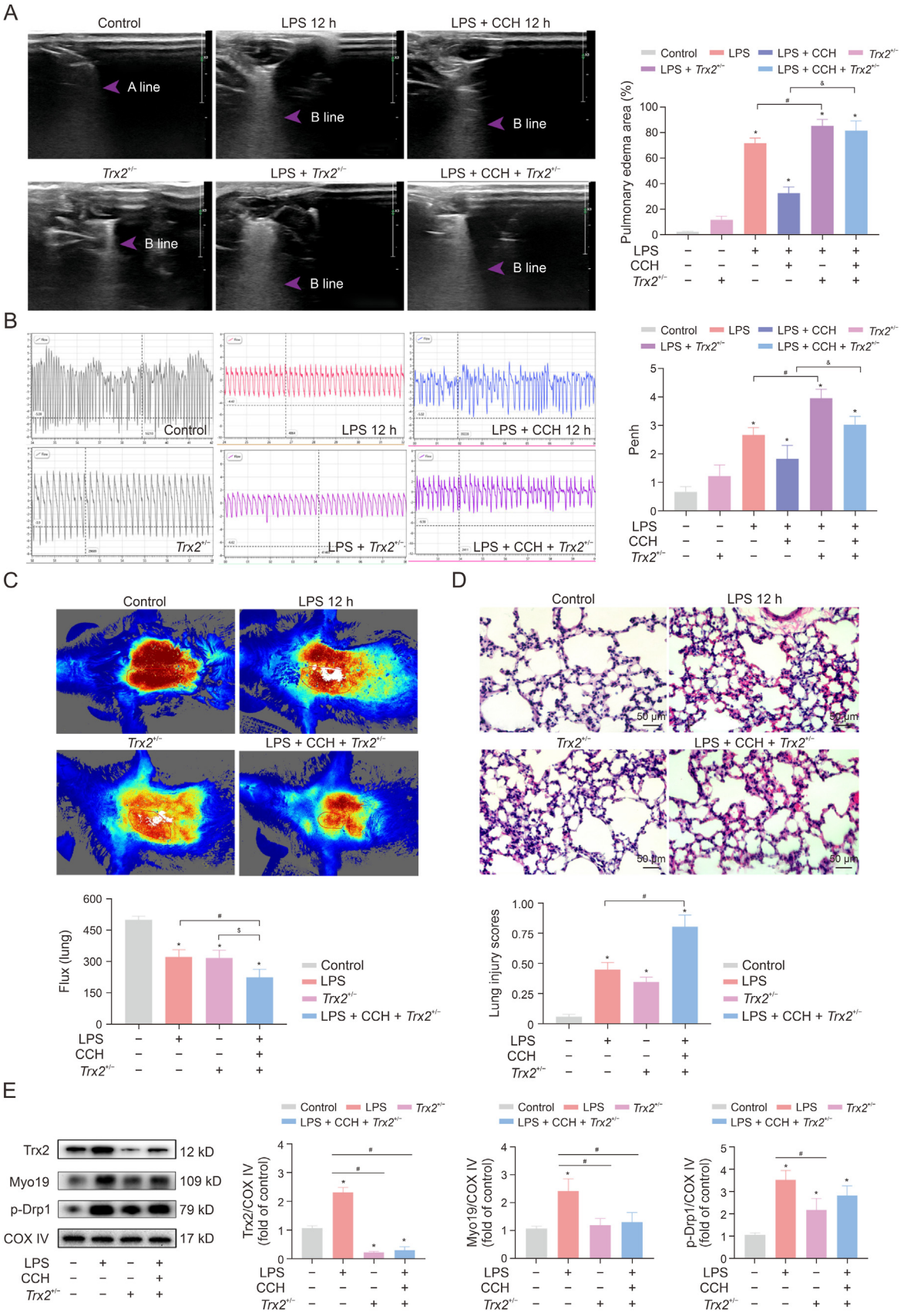

Fig. 6. Coral calcium hydrogenation (CCH) treatment of $Trx2^{+/-}$ lipopolysaccharide (LPS)-induced acute respiratory distress syndrome (ARDS) mice showed no improvement in acute lung injury. (A) The ultrasound examination images of lung tissue ($n = 3$ in each group). (B) The lung function test images of lung tissue ($n = 3$ in each group). (C) The Speckle Doppler detection of local pulmonary blood flow images of lung tissue ($n = 3$ in each group). (D) Representative images of hematoxylin and eosin (HE)-stained lung tissue sections

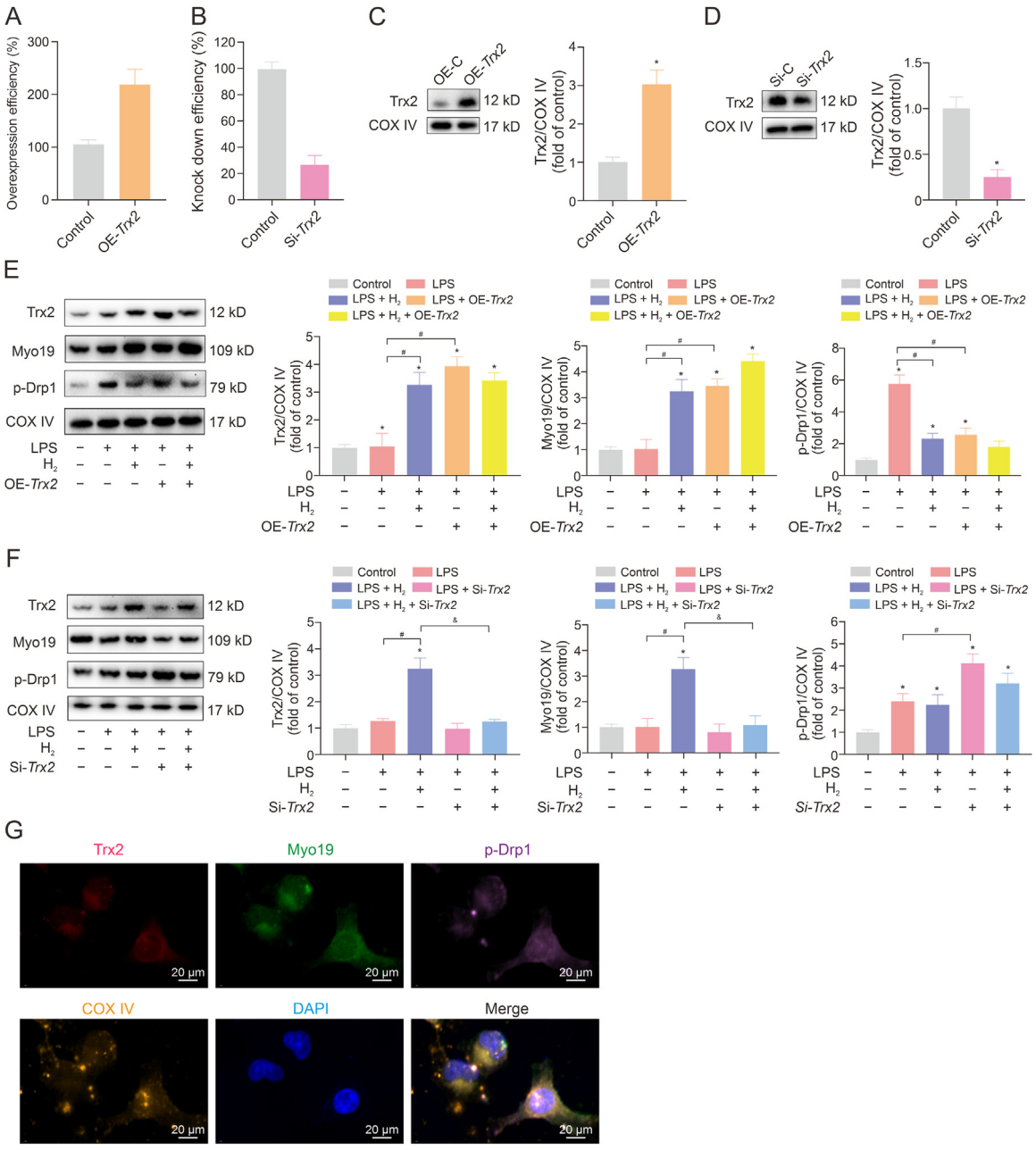

Fig. 7. Changes in Myo19/P-dynamin-related protein 1 (Drp1) in A549 cells were observed by overexpressing and silencing *Trx2*. (A) Quantitative polymerase chain reaction (q-PCR) analysis of *Trx2* mRNA expression with *Trx2*-containing plasmid transfection in A549 cells ($n = 3$ in each group). (B) qRT-PCR analysis of *Trx2* mRNA expression with *Trx2* knockdown plasmid transfection in A549 cells (n = 3 in each group). (C) Western blot analysis of Trx2 protein expression after transfected with *Trx2*-containing plasmid in A549 cells ($n = 3$ in each group). (D) Western blot analysis of Trx2 protein expression after transfecting *Trx2* knockdown plasmid in A549 cells ($n = 3$ in each group). (E) Representative images of Trx2, Myo19 and p-Drp1 expression detected by Western blotting after overexpression of *Trx2* for 12 h ($n = 3$ in each group). (F) Representative images of Trx2, Myo19, and p-Drp1 expression detected by Western blotting after knockdown of *Trx2* for 12 h ($n = 3$ in each group). (G) A549 cells were stained with immunofluorescence at 12 h, showing Trx2, Myo19 and p-Drp1 activation in the hydrogen-treated group. A significant difference was revealed by one-way analysis of variance (ANOVA). $^{*}P < 0.05$ versus control; $^{\#}P < 0.05$ versus lipopolysaccharide (LPS)-induced group; $^{\&}P < 0.05$ versus LPS-induced hydrogen therapy group. OE: overexpression; Si: small interfering; DAPI: 4',6-diamidino-2-phenylindole.

local mitochondrial clearance is complex. In addition to Drp1, which is a key effector protein in mitochondrial peripheral division, there is also an important initiator Myo19, which exerts a critical braking effect on local mitochondrial clearance, directly determining whether the mitochondria can successfully initiate peripheral division to scavenge the damaged mtDNA.

Myo19 localizes to the mitochondria through a 30–45-residue segment in its C-terminal tail domain upon stimulation by excessive ROS [34]. Studies have demonstrated that mitochondrial localization of Myo19 enables it to function as a regulator of cellular adaptive responses [35]. The aberrant increase in ROS levels allows Myo19 to sense damaged mtDNA at the tips of tubular

($n = 3$ in each group). (E) Mitochondrial purification of 12 h lung tissue. The expressions of Trx2, Myo19, and p-Drp1 were performed by Western blotting ($n = 3$ in each group). Data are presented as means ± standard deviation (SD), and were analyzed by one-way analysis of variance (ANOVA) followed by Bonferroni's post hoc test. $^{*}P < 0.05$ versus control; $^{\#}P < 0.05$ versus LPS-induced group. Drp1: dynamin-related protein 1.

mitochondria by altering the mitochondrial membrane potential and subsequently anchors it to actin filaments migrating towards the plasma membrane at the cell base. Myo19 can modulate the rate of mitochondrial division by regulating the activation of Drp1, which is crucial for maintaining mitochondrial homeostasis [36]. In this study, we observed a significant upward trend in Myo19 expression within 3 h after CCH treatment in ARDS mice, while ARDS mice without treatment showed a slower upward trend. Consistent results were obtained from *in vitro* cell experiments. These findings suggest that hydrogen gas promotes early-stage activation of local mitochondrial clearance mechanisms through mediating Myo19 activation. Given that previous studies have shown that ROS content regulates *in vivo* activation of Myo19, we speculate that hydrogen gas enhances Myo19 activation via regulation of ROS levels, and this regulation is closely associated with the REDOX reaction system.

The Trx system is a key regulatory system for *in vivo* REDOX reactions, capable of mitigating the abnormal increase in ROS by activating AMPK, Nrf-2, MAPK, and other pathways [37,38]. In mammals, the Trx system comprises Trx1 and Trx2. Trx1 is exclusively expressed in the cytoplasm of cells, while Trx2 is solely expressed in the mitochondria. However, both Trx1 and Trx2 play crucial roles in regulating substrate REDOX state and providing antioxidant protection. Therefore, they represent important potential therapeutic targets for oxidative-stress-related diseases. In this study, we observed rapid upregulation of mitochondrial Trx2 3 h after CCH hydrogen release in ARDS mice, while upregulation of Trx2 mice was slower. These trends were confirmed by *in vitro* cell experiments. we noted an upward trend of Trx2 and Myo19 in control mice treated with CCH alone. We hypothesized that hydrogen may affect the activation of Myo19 and P-Drp1 through upregulation of Trx2. In $Trx2^{+/-}$ mice, the protective effect of CCH on ARDS almost disappeared. Furthermore, these mice became more susceptible to LPS-induced ARDS lung injury. Wester blotting immunoprecipitation analysis revealed that expression of Myo19 and P-Drp1 was inhibited in $Trx2^{+/-}$ mice; however, the change in trend was more pronounced for Myo19 than for P-Drp1. Plasmid and siRNA transfection techniques were used to conduct Trx2 overexpression and gene silencing in A549 cells *in vitro*. After Trx2 overexpression, Myo19 and P-Drp1 showed an upregulation trend, although this was less pronounced for P-Drp1. Conversely, upon Trx2 silencing, Myo19 was significantly inhibited but downregulation of P-Drp1 was not as evident. The results obtained from *in vitro* and *in vivo* experiments corroborated our hypothesis regarding the impact of Trx2 on Myo19/P-Drp1. The trends in expression of P-Drp1 were less pronounced compared with those of Trx2 and Myo19, which may be attributed to the delayed expression of P-Drp1 in comparison with Trx2 and Myo19. Unilateral factors of Trx2/Myo19 should not affect the *in vivo* activation of P-Drp1. The intricate protein networks also influenced expression of Myo19 and Drp1. However, this study did not extensively investigate the mechanism by which Trx2 regulates Myo19 or identify the target responsible for hydrogen-specific upregulation of Trx2. These aspects will be further explored in our future research.

5. Conclusion

This study demonstrates that CCH, functioning as a solid molecular hydrogen carrier, effectively mitigates acute lung injury in ARDS mice by releasing hydrogen following oral administration. Hydrogen therapy for ARDS-induced acute lung injury is closely associated with the early promotion of mitochondrial fission in AT II cells. The mechanism underlying hydrogen-induced peripheral division of mitochondria involves the activation of key genes Myo19/P-Drp1 mediated by upregulation of mitochondrial Trx2.

CRediT authorship contribution statement

Qian Li: Writing – original draft. **Yang Ang:** Writing – review & editing. **Qing-Qing Zhou:** Data curation. **Min Shi:** Investigation. **Wei Chen:** Methodology. **Yujie Wang:** Software. **Pan Yu:** Supervision. **Bing Wan:** Validation. **Wanyou Yu:** Visualization. **Liping Jiang:** Formal analysis. **Yadan Shi:** Methodology. **Zhao Lin:** Project administration. **Shaozheng Song:** Funding acquisition, Writing – review & editing. **Manlin Duan:** Conceptualization, Funding acquisition. **Yun Long:** Formal analysis, Funding acquisition. **Qi Wang:** Funding acquisition, Resources, Writing – review & editing. **WenTao Liu:** Funding acquisition, Project administration. **Hongguang Bao:** Funding acquisition, Methodology.

Declaration of competing interest

The authors declare that there are no conflicts of interest.

Acknowledgments

This work was supported by the Nanjing Medical Science and Technology Development Project, China (Project No.: YKK23221), Open Project of Immune Cell Translational Research Center of Jiangning Hospital, Nanjing Medical University, China (Project No.: JNYYZXKY202216), General Project of Medical Education Collaborative Innovation Fund of Jiangsu University, China (Project No.: JDYY2023094), China Red Cross Foundation Medical Empowerment Charity Special Fund Project (Project No.: CRCF-YXFN-202302028). We thank International Science Editing (http://www.internationalscienceediting.com) for editing this manuscript. We would like to thank Ms. Xi-wen Yao from Shandong Rizhao Life Valley Biotechnology Co., Ltd. (Rizhao, Shandong, China) for providing the coral calcium hydride.

Appendix A. Supplementary data

Supplementary data to this article can be found online at:https://doi.org/10.1016/j.jpha.2024.101039.

References

[1] E.A. Gorman, C.M. O'Kane, D.F. McAuley, Acute respiratory distress syndrome in adults: Diagnosis, outcomes, long-term sequelae, and management, Lancet 400 (2022) 1157–1170.
[2] M.C.J. Kneyber, R.G. Khemani, A. Bhalla, et al., Understanding clinical and biological heterogeneity to advance precision medicine in paediatric acute respiratory distress syndrome, Lancet Respir. Med. 11 (2023) 197–212.
[3] G. Grasselli, C.S. Calfee, L. Camporota, et al., ESICM guidelines on acute respiratory distress syndrome: Definition, phenotyping and respiratory support strategies, Intensive Care Med. 49 (2023) 727–759.
[4] J. Hadaya, P. Benharash, Prone positioning for acute respiratory distress syndrome (ARDS), JAMA 324 (2020), 1361.
[5] D. Wang, H. Liu, S. Bai, et al., The PAR6B-PRKCI-PAR3 complex influences alveolar regeneration in patients with the emphysema subtype of chronic obstructive pulmonary disease, Stem Cell Res. Ther. 16 (2025), 97.
[6] J. Dutra Silva, Y. Su, C.S. Calfee, et al., Mesenchymal stromal cell extracellular vesicles rescue mitochondrial dysfunction and improve barrier integrity in clinically relevant models of ARDS, Eur. Respir. J. 58 (2021), 2002978.
[7] S. Robichaud, V. Rochon, C. Emerton, et al., Trehalose promotes atherosclerosis regression in female mice, Front. Cardiovasc. Med. 11 (2024), 1298014.
[8] H. Jiao, D. Jiang, X. Hu, et al., Mitocytosis, a migrasome-mediated mitochondrial quality-control process, Cell 184 (2021) 2896–2910.e13.
[9] T. Kleele, T. Rey, J. Winter, et al., Distinct fission signatures predict mitochondrial degradation or biogenesis, Nature 593 (2021) 435–439.
[10] N. Li, R. Xiong, G. Li, et al., A novel mechanism for the protection against acute lung injury by melatonin: Mitochondrial quality control of lung epithelial cells is preserved through SIRT3-dependent deacetylation of SOD2, Cell. Mol. Life Sci. 79 (2022), 610.
[11] Q. Li, P. Yu, Q. Zeng, et al., Neuroprotective effect of hydrogen-rich saline in global cerebral ischemia/reperfusion rats: Up-regulated tregs and down-regulated miR-21, miR-210 and NF-κB expression, Neurochem. Res. 41 (2016) 2655–2665.

[12] Y. Ueda, A. Nakajima, T. Oikawa, Hydrogen-related enhancement of *in vivo* antioxidant ability in the brain of rats fed coral calcium hydride, Neurochem. Res. 35 (2010) 1510–1515.
[13] C. Hou, Y. Wang, E. Zhu, et al., Coral calcium hydride prevents hepatic steatosis in high fat diet-induced obese rats: A potent mitochondrial nutrient and phase II enzyme inducer, Biochem. Pharmacol. 103 (2016) 85–97.
[14] A. Andor, M. Mohanraj, Z.A. Pató, et al., TXNL1 has dual functions as a redox active thioredoxin-like protein as well as an ATP- and redox-independent chaperone, Redox Biol. 67 (2023), 102897.
[15] C. Guerra, M. Molinari, Thioredoxin-related transmembrane proteins: TMX1 and little brothers TMX2, TMX3, TMX4 and TMX5, Cells 9 (2020), 2000.
[16] D.P. Ball, L.P. Tsamouri, A.E. Wang, et al., Oxidized thioredoxin-1 restrains the NLRP1 inflammasome, Sci. Immunol. 7 (2022), eabm7200.
[17] G. He, K. Chen, H. Wang, et al., Fudosteine attenuates acute lung injury in septic mice by inhibiting pyroptosis *via* the TXNIP/NLRP3/GSDMD pathway, Eur. J. Pharmacol. 926 (2022), 175047.
[18] J. Li, S. Ruan, J. Jia, et al., Hydrogen attenuates postoperative pain through Trx1/ASK1/MMP9 signaling pathway, J. Neuroinflammation 20 (2023), 22.
[19] M. Mathru, A-lines and B-lines: Lung ultrasound as a bedside tool for predicting pulmonary artery occlusion pressure in the critically ill, Yearb. Anesthesiol. Pain Manag. 2010 (2010) 215–216.
[20] D.A. Lichtenstein, P. Mauriat, Lung ultrasound in the critically ill neonate, Curr. Pediatr. Rev. 8 (2012) 217–223.
[21] D.A. Lichtenstein, BLUE-protocol and FALLS-protocol: Two applications of lung ultrasound in the critically ill, Chest 147 (2015) 1659–1670.
[22] G. Matute-Bello, G. Downey, B.B. Moore, et al., An official American thoracic society workshop report: Features and measurements of experimental acute lung injury in animals, Am. J. Respir. Cell Mol. Biol. 44 (2011) 725–738.
[23] I. Ohsawa, M. Ishikawa, K. Takahashi, et al., Hydrogen acts as a therapeutic antioxidant by selectively reducing cytotoxic oxygen radicals, Nat. Med. 13 (2007) 688–694.
[24] Y. Long, Y. Ang, W. Chen, et al., Hydrogen alleviates impaired lung epithelial barrier in acute respiratory distress syndrome *via* inhibiting Drp1-mediated mitochondrial fission through the Trx1 pathway, Free. Radic. Biol. Med. 218 (2024) 132–148.
[25] Y. Ueda, T. Kojima, T. Oikawa, Hippocampal gene network analysis suggests that coral calcium hydride may reduce accelerated senescence in mice, Nutr. Res. 31 (2011) 863–872.
[26] X. Wang, B. Tong, R. Hui, et al., The role of hyperthermia in methamphetamine-induced depression-like behaviors: Protective effects of coral calcium hydride, Front. Mol. Neurosci. 14 (2022), 808807.
[27] Q. Li, M. Shi, Y. Ang, et al., Hydrogen ameliorates endotoxin-induced acute lung injury through AMPK-mediated bidirectional regulation of Caspase3, Mol. Immunol. 168 (2024) 64–74.
[28] B. Ruaro, F. Salton, L. Braga, et al., The history and mystery of alveolar epithelial type II cells: Focus on their physiologic and pathologic role in lung, Int. J. Mol. Sci. 22 (2021), 2566.
[29] K.D. Wick, A. Leligdowicz, H. Zhuo, et al., Mesenchymal stromal cells reduce evidence of lung injury in patients with ARDS, JCI Insight 6 (2021), e148983.
[30] Y. Cui, Y. Li, S. Meng, et al., Molecular hydrogen attenuates sepsis-induced cardiomyopathy in mice by promoting autophagy, BMC Anesthesiol. 24 (2024), 72.
[31] N. Lian, X. Mao, Y. Su, et al., Hydrogen-rich medium ameliorates lipopolysaccharides-induced mitochondrial fission and dysfunction in human umbilical vein endothelial cells (HUVECs) *via* up-regulating HO-1 expression, Int. Immunopharmacol. 110 (2022), 108936.
[32] V. Garrido-Bazán, J.P. Pardo, J. Aguirre, DnmA and FisA mediate mitochondria and peroxisome fission, and regulate mitochondrial function, ROS production and development in *Aspergillus nidulans*, Front. Microbiol. 11 (2020), 837.
[33] J. Yang, L. Liu, Y. Oda, et al., Highly-purified rapidly expanding clones, RECs, are superior for functional mitochondrial transfer, Stem Cell Res. Ther. 14 (2023), 40.
[34] B.I. Shneyer, M. Ušaj, A. Henn, Myo19 is an outer mitochondrial membrane motor and effector of starvation-induced filopodia, J. Cell Sci. 129 (2016) 543–556.
[35] A.J. Kruppa, F. Buss, Motor proteins at the mitochondria-cytoskeleton interface, J. Cell Sci. 134 (2021), jcs226084.
[36] K. Majstrowicz, U. Honnert, P. Nikolaus, et al., Coordination of mitochondrial and cellular dynamics by the actin-based motor Myo19, J. Cell Sci. 134 (2021), jcs255844.
[37] J. Muri, M. Kopf, Redox regulation of immunometabolism, Nat. Rev. Immunol. 21 (2021) 363–381.
[38] J. Muri, H. Thut, Q. Feng, et al., Thioredoxin-1 distinctly promotes NF-κB target DNA binding and NLRP3 inflammasome activation independently of Txnip, Elife 9 (2020), e53627.